# A PERSONAL-COMPUTER-BASED IMAGING STOKES POLARIMETER FOR SOLAR OBSERVATIONS

A. V. ANANTH, P. VENKATAKRISHNAN, R. S. NARAYANAN, and J. C. BHATTACHARYYA
*Indian Institute of Astrophysics, Bangalore 560034, India*

(Received 6 September, 1993; in revised form 7 January, 1994)

**Abstract.** For measurements of vector magnetic field over solar active regions, a Stokes polarimeter for studying the polarisation profiles on selected spectral lines is described. This paper gives details of the relevant CCD imaging system and the personal computer (PC)-based acquisition, together with the image analysis techniques necessary for the task. Field trials and tests of the system are also described.

## 1. Introduction

The Zeeman broadening of magnetically sensitive spectral lines formed in the solar atmosphere produces a characteristic polarisation signature. This signature can be used for estimating the strength and orientation of solar magnetic fields (Harvey, 1984). Basically, two schemes can be adopted. In one scheme, a 2D image of a region of the Sun is recorded in various polarisations using narrow-band filters tuned to the wings of the spectral lines (Hagyard *et al.*, 1982; Zirin, 1985; Ai, 1987; Makita, Hamana, and Nishi, 1985; Rust and O'Byrne, 1991; Lundstedt *et al.*, 1991; Title, Tarbell, and Topka, 1987). In another scheme, a 1D region of the Sun is imaged onto the slit of a spectrograph, which disperses the light in an orthogonal direction to produce a 2D image (Micky, 1985; Lites *et al.*, 1991; Jones *et al.*, 1992). The key component in either scheme is an imaging polarimeter.

The latter scheme has been chosen by us chiefly because of the availability of a high-dispersion spectrograph at Kodaikanal for solar spectroscopy (Bappu, 1961). The availability of personal computers of substantial capabilities, charge coupled device (CCD) cameras, and high-speed frame grabbing units at affordable cost enabled us to build an imaging polarimeter as a back-end instrument for the solar tower/tunnel telescope at Kodaikanal.

## 2. Instrument Description

The major subsystems of the experimental set up are: (i) the telescope; (ii) a dispersing spectrograph; (iii) a polarimeter which analyses the light; (iv) the CCD camera which records the spectra; and (v) a PC based data acquisition and processing system for CCD images.

The telescope is a 3-mirror coelostat system that directs the sunlight onto a 38-cm lens of 36 m focal length that produces a 34-cm image of the Sun at the focal

*Solar Physics* **151:** 231–241, 1994.

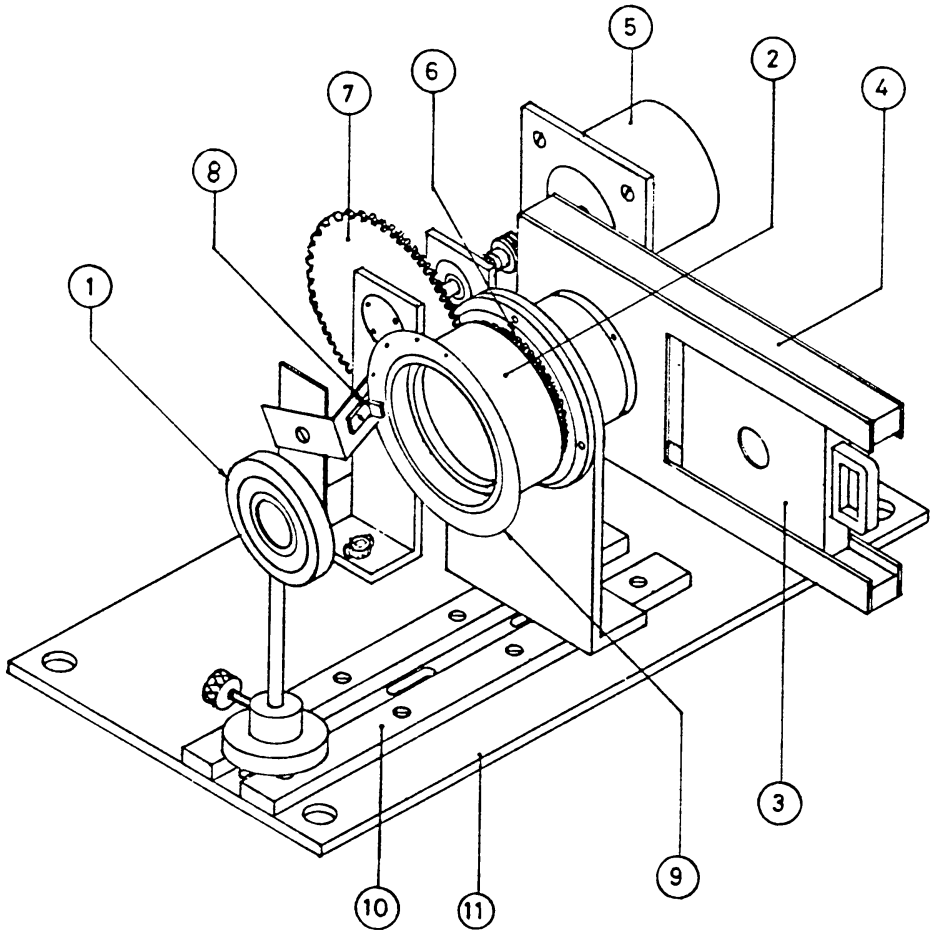


Fig. 1. The polarimeter configuration is shown. Various parts are numbered as follows: (1) analyser holder, (2) rotatable retarder plate holder, (3) insertable quarterwave plate holder (optional), (4) quarter wave plate carrier, (5) stepper motor, (6) 40 teeth spur gear, (7) 100 teeth spur gear, (8) IR source and sensor assembly, (9) mounting disc for IR source and sensor, (10) rails for alignment, (11) base plate.

plane. The polarimeter analyses the light a little ahead of the focus. The analyzed light passes through the entrace slit of the 60 foot long spectrograph. The grating is mounted in the Littrow arrangement, and the spectrum is imaged at the exit slit of the spectrograph. The CCD camera is mounted at this position. The video output from the camera is frame grabbed, and the digitized data is stored in the PC. The telescope and spectrograph details are described elsewhere (Bappu, 1961).

### 2.1. THE PC-CONTROLLED POLARIMETER

The modulator is a rotating retarder plate (Figure 1) that has quarter wave retardation at 630.2 nm. A slo-syn (M61) stepper motor drives the retarder plate through a 100:40 gear train. The motor is driven at a speed of 0.5 rev $s^{-1}$. The least count of the motor is 1.8° at the shaft, resulting in 4.5° for the retarder plate.

The analyser is a polarizing prism that separates the light into two beams of orthogonal polarisations. The ordinary or *o*-beam is undeviated and reaches the

grating of the spectrograph. The extraordinary or $e$-beam, deviated by 6.3°, is not used precisely. The analyser transmission axis is kept aligned with the spectrograph slit and serves as the reference $X$-axis for the Stokes parameter system.

The analyser is mounted on rails so that the gap between the analyser and retarder can be varied while maintaining the alignment. This feature is useful in the initial stages when the system is under testing.

The retarder plate movement was made smooth by employing needle bearings. The movement of the plate is unidirectional and hence immune to backslash of the gears. The plate is always brought to a reference point, which is identified by an IR source sensor pair which is mounted on the plate holder. The polarimeter is itself mounted on an accurately machined base plate and fixed to a stand, whose tilt is adjustable by means of studs.

An intelligent controller for driving the stepper motor was designed and fabricated locally. This card has the following features: (1) a provision for selection of clock speeds; (2) forward/reverse motion selection; (3) number of steps selection.

The computer loads these parameters and is thereafter free to perform other operations while the controller independently drives the motor.

### 2.2. THE CCD CAMERA

The detector is a CCD-based camera containing a P46380 scientific grade chip from EEV, U.K. The camera is an asynchronous Peltier cooled system and can operate in any one of the following three modes: (a) standard video mode; (b) 1 ms exposure (electronically shuttered) mode; and (c) asynchronous mode.

It is the asynchronous mode that is used for this particular application. In this mode, one chip integration is possible for about 5 s. The upper limit is set by the dark current. Even this is possible only because of Peltier cooling, which maintains the chip at 40 °C below the ambient temperature. The CCD chip has $365 \times 576$ pixels each $22\mu \times 22\mu$ in size. However, the actual exposed area is only $385 \times 288$ pixels since half the chip is used as an image store. The quoted S/N ratio at a peak illumination of 1–3 lux is 55 db. The camera responds to light in the spectral range between 450 nm and 1000 nm with a peak response at 600 nm.

In the normal TV mode operation, the charges generated in the 20 ms time available between the 'sync' pulses, are quickly transferred to the image store portion of the CCD (the 288 rows) within 100 $\mu$s. The charges are then read out during the next 20 ms cycle into a standard CCIR video format interlaced with a previous 20 ms field. This output can then be directly interfaced with a TV display or VCR or a video frame-grabber unit. For our light levels, this mode was found to be inadequate, and hence we had to switch to the asynchronous mode of operation.

In the asynchronous mode, the instant and duration of on-chip integration can be controlled externally. The photo charges generated during every 20 ms cycle is reverse clocked into a diode drain at the top of the sensor. This acts as a unique electronic shutter, a technique patented by EEV, the camera manufacturers. A strobe pulse is applied during which the reverse clocking is halted and the image is

integrated onto the chip. The pulse width determines the exposure time. After the exposure, the charges are transferred to the image store portion, where it is available for read-out in the next 20 ms cycle. The camera generates a frame-available signal which is used to indicate the frame store when an image from the camera can be frame grabbed.

The camera itself is mounted at the exit slit of the spectrograph using a specially fabricated camera holding unit. This unit has provisions for lateral, forward, and tilt motions. All these (except the lateral motion) are controlled mechanically by screws. The forward motion is required for arriving at the focal plane, the tilt is needed to align the CCD rows with the direction of spectral dispersion, the swivelling is necessary to square the camera and to remove fringes that appear due to internal reflection of light in the CCD substrate.

### 2.3. The PC-based Image Data Acquisition and Processing System

The diagram of the electronic system is as shown in Figure 2. The video output is digitized and stored on a $512 \times 512$, 8-bit frame buffer using the DT-2861 card that resides on the expansion slot of the IBM compatible PC/AT. This card has 16 such buffers available on board. The total time required to acquire and store each image on the frame buffer was found to be $\sim$170 ms. A companion DT-2858 arithmetic processor card allows simple arithmetic operations on the image with 16-bit accuracy.

### 2.4. Data Back Up on Magnetic Tape

A 9-track $\frac{1}{2}$-inch magnetic tape is available for data back up and porting to other systems for further analysis of the data.

### 2.5. Software Description

The control of various operations of the camera, polarimeter, and data acquisition is performed using a specially written package that uses FORTRAN as well as ASSEMBLY programmes in a DOS environment.

The main features of the software package are: (1) image acquisition; (2) file/buffer handling; (3) simple functions for on-line quick look analysis.

The software also makes use of a callable library DT-IRIS for frame buffer related operations.

The assembly language routines have been used for: (1) speeding up input/output operations; (b) handling interrupts; (c) controlling screen functions.

The CCD on-chip integration timings are derived from the PC timer. The PC timer 'O' registers have been reprogrammed and control over (1C Hex) interrupt vector taken over by the application.

The flow chart of the software for acquisition is given in Figure 3.

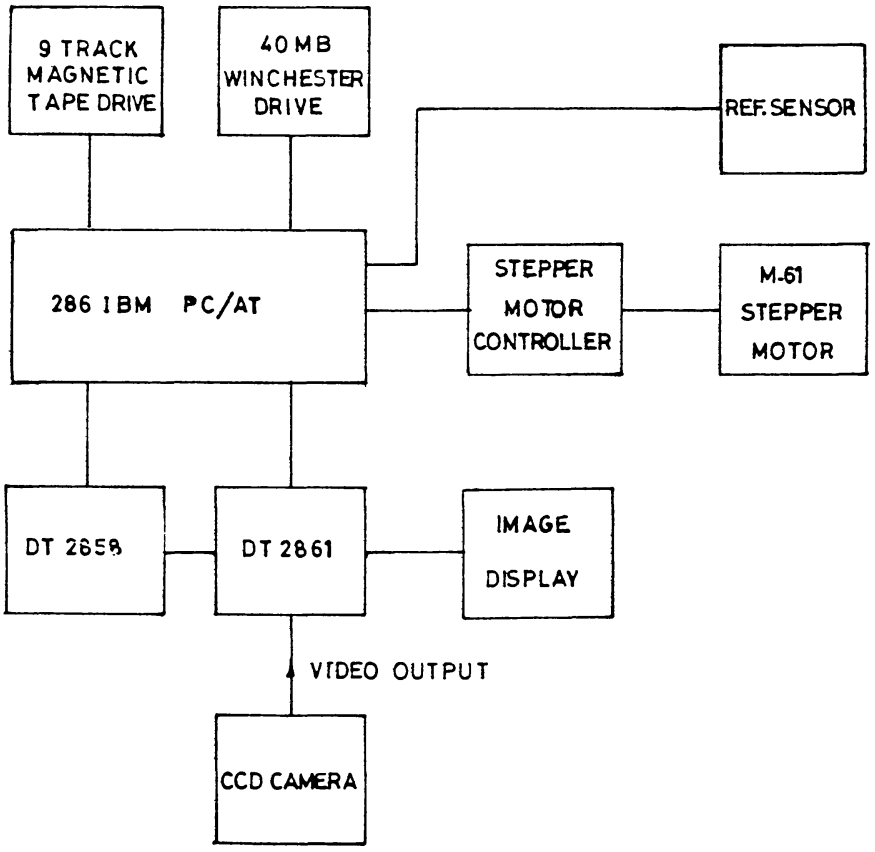


Fig. 2. Schematic diagram of the electronics is shown. The various subsystems are indicated within the boxes.

## 3. Performance Evaluation at the Site

The modulated output through the analyser is given by (Makita, Hamana, and Nishi, 1985)

$$I(\theta) = \tfrac{1}{2}[I_0 + \tfrac{1}{2}(1 + \cos\delta)Q_0 + \tfrac{1}{2}(1 - \cos\delta)\,(Q_0 \cos 4\theta + U_0 \sin 4\theta) + \\ + V_0 \sin\delta \sin 2\theta]\,, \qquad (1)$$

where $\theta$ is the angle made by the fast axis of the retarder plate to the transmission axis of the analyser, reckoned positive when measured clockwise as viewed in the direction of light propagation. $I_0$, $Q_0$, $U_0$, and $V_0$ are the Stokes parameters that characterize the polarisation of the beam, and $\delta$ is the retardation of the modulator. The scheme adopted for this polarimeter is to record several frames at different values of $\theta$ and perform a least-squares fit to Equation (1). This scheme is more general in nature and is not dependent on $\delta$. Thus any spectral region can be chosen at will. Schemes using subtraction of frames recorded at particular values of $\theta$ for fixed $\delta$, would not work at different wavelengths unless achromatic retarders are employed. These are very expensive. For the spectral region of our

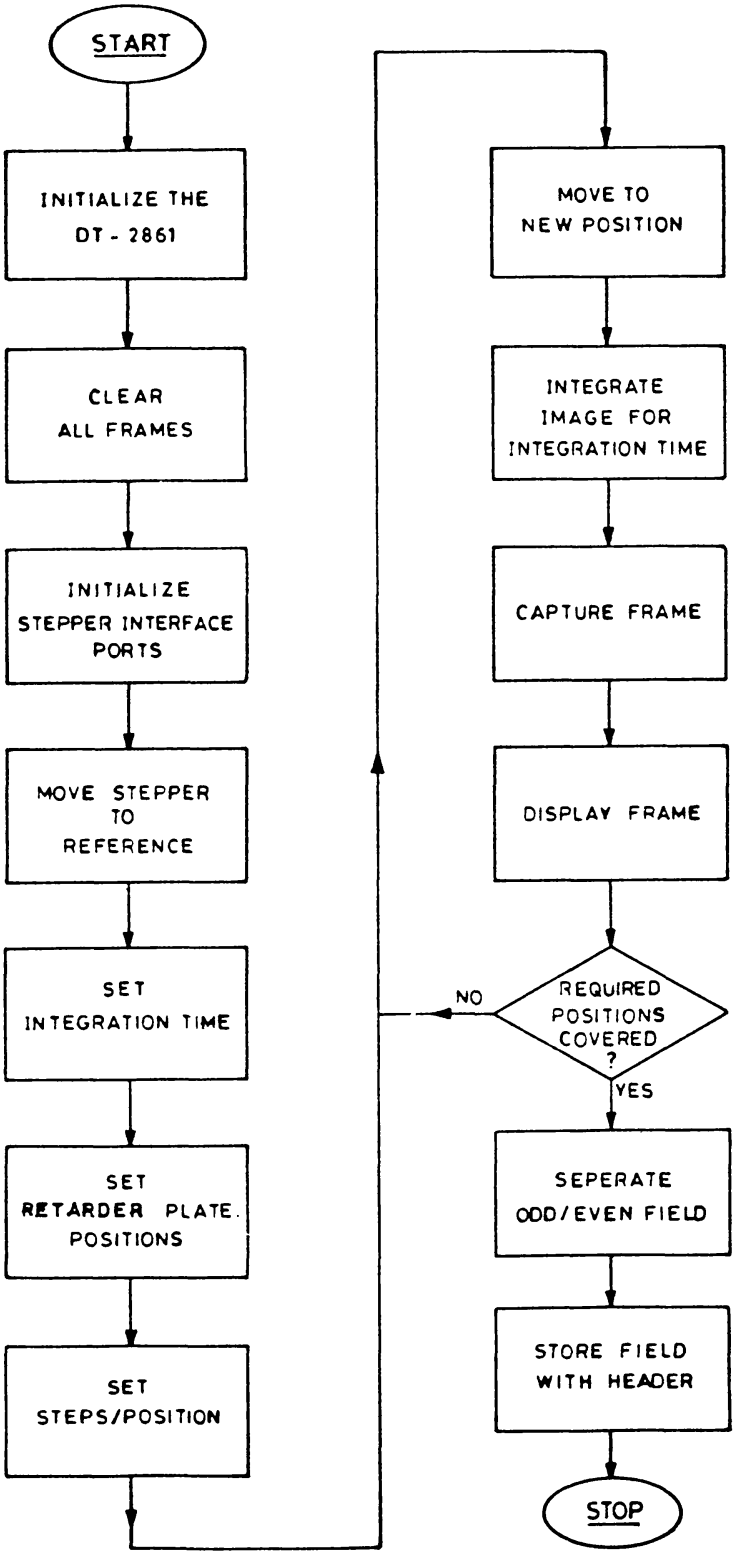


Fig. 3. The flow chart of the software for data acquisition is shown. All steps are sequential, but stepper motor control is done independently once the parameters of motor movement are loaded into the motor controller. The computer moves on to the next task but checks the position of the retarder plate before giving the acquire frame command to the frame grabber card. The rest of the commands are done sequentially.

interest (630 nm), the $\delta$ of the retarder is $\pi/2$. The polarimeter performance was checked for the following parameters: (a) sensitivity of polarisation measurements; (b) uniformity over the area of detection; (c) level of cross-talk between linear and circular polarisations.

The origin of cross-talk between linear and circular polarisations is retardation errors in the waveplate. We therefore allowed light of a fixed linear polarisation to pass through the polarimeter. The least-squares fit was performed to Equation (1) with $V_0$ assumed to be zero. The residuals after the fit would then give an upper limit to the cross-talk between linear and circular polarisations. We then assumed that the cross-talk from circular to linear polarisation would be of the same order. We did not separately perform the test for input circular polarisation, chiefly because of the difficulty of generating standard sources of exact circular polarisation. The sunlight was used as the illuminating source and a polaroid sheet inserted into the path of sunlight before entering the polarimeter served to generate the linear polarisation.

The modulator was stepped through 10 positions at 9° per step. The exposure times were of the order of a few seconds. For each setting of the input polariser, the exposure time was fixed. The entrance slit was 100$\mu$. The grating was oriented to diffract the second order at 630 nm into the camera. An OG-10 filter was placed before the entrance slit to suppress the higher orders. The lower first order at 1.26 $\mu$m is automatically precluded due to the insensitivity of the CCD camera in this spectral region. The resulting spectra were least-square fitted to Equation (1) to obtain the Stokes parameters. The Stokes parameter evaluation required simultaneous access to 15 images each 256 $\times$ 512 in size. Flat fielding was not performed since we are basically interested in intensity ratios at each pixel for the purposes of this study. The stray light, along with the bias and dark counts amounted to a total of 2 to 3 counts as seen in the image of the crosswire. For the signal level used in the present analysis, this contribution was not significant. In general, the counts in the image of the crosswire will provide a handle on the background of stray-light+bias+dark. This is especially useful in view of the fact that the combination of commercial TV cameras and frame grabbers would have inherent problems in the d.c. restoration during frame grabbing operations. This measure of the background is subject to errors caused by its variation across the entire frame. Integrating the signal for sufficiently high levels is one way of minimising these errors. Use of the polarized components, $Q_0$, $U_0$, and $V_0$ alone and avoiding the total light, $I_0$, in the line profile analysis, as advocated in Skumanich and Lites (1987), is yet another way of tackling this problem.

A curious, albeit small, correlation of $Q_0/I_0$ and $U_0/I_0$ with $I_0$ was seen in the results. This could be due to a small nonlinearity in the response of the CCD-frame-grabber combination. We have therefore also estimated the coefficient of correlation of $Q_0/I_0$ and $U_0/I_0$ with $I_0$. The correlation of the residuals with $I_0$ is also given. Table I shows the results for two settings of the input polariser. The descriptions of the various columns are given below the table.

TABLE I
Evaluation of polarimeter performance

| 1 | 2 | 3 | 4 | 5 | 6 | 7 | 8 | 9 | 10 | 11 | 12 |
|---|---|---|---|---|---|---|---|---|---|---|---|
| 6 May, 1993 $5^h52^m$ | 46 800 | −54 | 77 | 0.99 | 0.01 | −0.005 | 0.0001 | 20 | 0.7 | 1.3 | 0.3 |
| 8 May, 1993 $5^h52^m$ | 47 850 | – | 101 | 1.40 | – | −0.020 | −0.0005 | 30 | – | 2.4 | 1.0 |

(1) Date and time in UT of the observations.
(2) Total number of pixels considered for analysis.
(3) $Q_0/I_0$ in percent.
(4) $U_0/I_0$ in percent.
(5) Mean residual for individual pixel in percent.
(6) Coefficient of correlation of $Q_0/I_0$ with $I_0$ in percent count$^{-1}$.
(7) Coefficient of correlation of $U_0/I_0$ with $I_0$ in percent count$^{-1}$.
(8) Coefficient of correlation residuals with $I_0$ in percent count$^{-1}$.
(9) r.m.s. spread in total intensity $I_0$ in counts.
(10) r.m.s. spread in $Q_0/I_0$ in percent after removing correlation with $I_0$.
(11) r.m.s. spread in $U_0/I_0$ in percent after removing correlation with $I_0$.
(12) r.m.s. spread in residuals in percent after removing correlation with $I_0$.

Four important points to note are: (a) mean residual error in pixels is $\simeq 1\%$; (b) the worst possible cross-talk from linear to circular polarisation is limited to this residual error; (c) the r.m.s. spread of $Q_0/I_0$ and $U_0/I_0$ is limited to 2%; (d) $Q_0/I_0$ and $U_0/I_0$ have small correlations with $I_0$ in the region of 0.005% to 0.02% per count.

Finally, to test the ability of the system to detect circular polarisation, the $(I_0 + V_0)$ and $(I_0 - V_0)$ spectra of a sunspot were recorded. These data have not been corrected for the telescope polarisation, which has been theoretically modelled in some detail (Balasubramaniam, Venkatakrishnan, and Bhattacharyya, 1985). Figures 4 and 5 show the $I_0$ profile with the corresponding $V_0$ profiles for two positions on a sunspot. The systematic decrease in $I_0$ at the edges could be due to a variety of reasons including vignetting of light at the entrance of the camera. Flat fielding can perhaps remove these trends in the total intensity, $I_0$. The fluctuation in $V_0/I_0$ away from the Zeeman sensitive lines at 630.25 nm is only $\simeq \pm 1\%$, while the modulation within the lines is $\approx 20\%$ and $\approx 7\%$ respectively at the two positions, but the width of the splitting is the same. This denotes the same total field strength but decreasing line-of-sight component. The random fluctuation of $V_0/I_0$ in the spectral continuum is also of the same order as the residual fluctuation in the least-squares fit given in Table I.

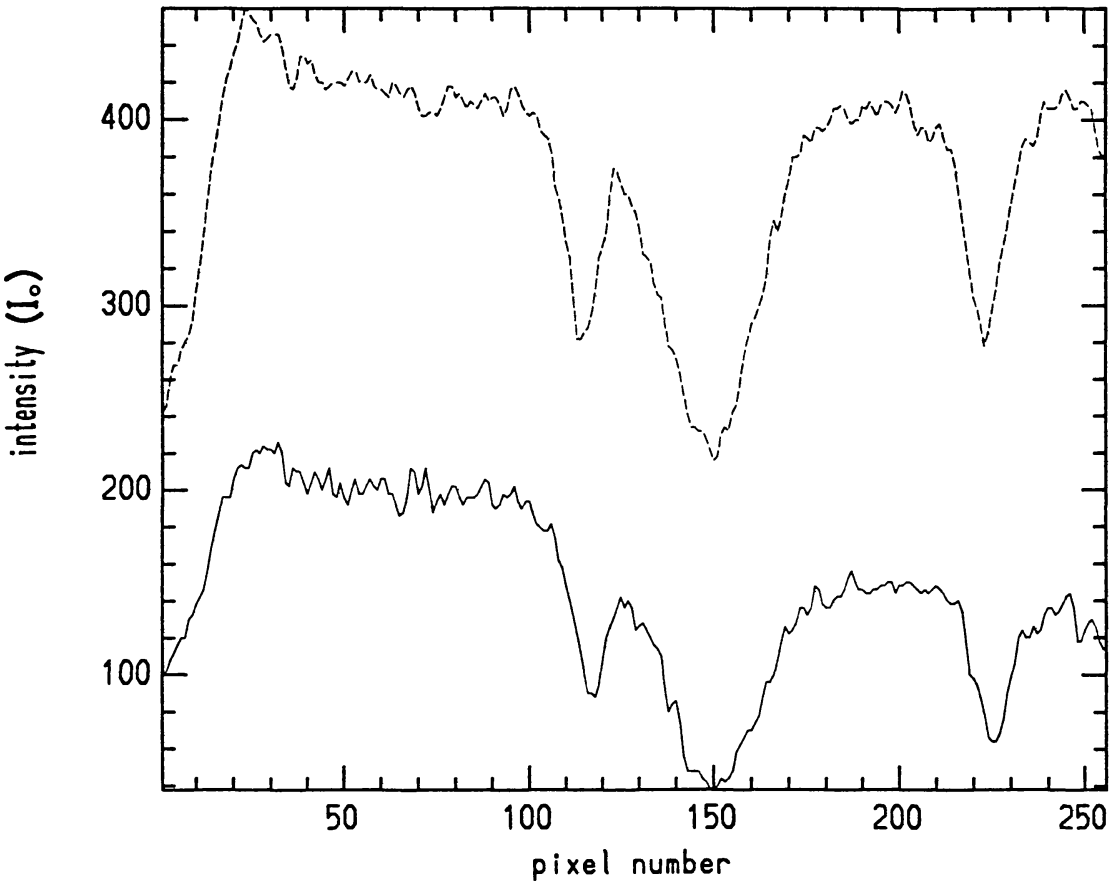


Fig. 4. The variation of intensity as a function of the pixel number. The two curves are at two different positions of a sunspot. One pixel equals 3 mÅ.

## 4. Discussion and Conclusions

The accuracy of 1% to 2% in the Stokes parameter measurements over a wide range of ~40 000 pixels is to be noted. Other instruments (Hagyard *et al.*, 1982) employing a wider spectral bandwidth (125 mÅ of the present instrument) have achieved accuracies of 0.01% after 256 enhancements. The wider bandwidth of these other instruments causes averaging over positive and negative values of the Stokes parameter variation along the line profile and this reduces the polarisation signal.

Our system thus has not only a greater signal to detect at an individual spectral position, but can use the systematic variation of the signal over several spectral positions to improve the overall sensitivity to detect magnetic fields. The binning of 25 spatial pixels to match the smearing produced by atmospheric 'seeing' will further increase the sensitivity. The Zeeman splitting of the lines in strong-field regions will also provide a proper calibration for the field strength.

Figures 4 and 5 show that the Zeeman splitting corresponds to a total field strength of 3000 G. The line-of-sight component of this field produces a $V_0/I_0$ amplitude of ≈20% at one location. The fluctuations in $V_0/I_0$ away from the line

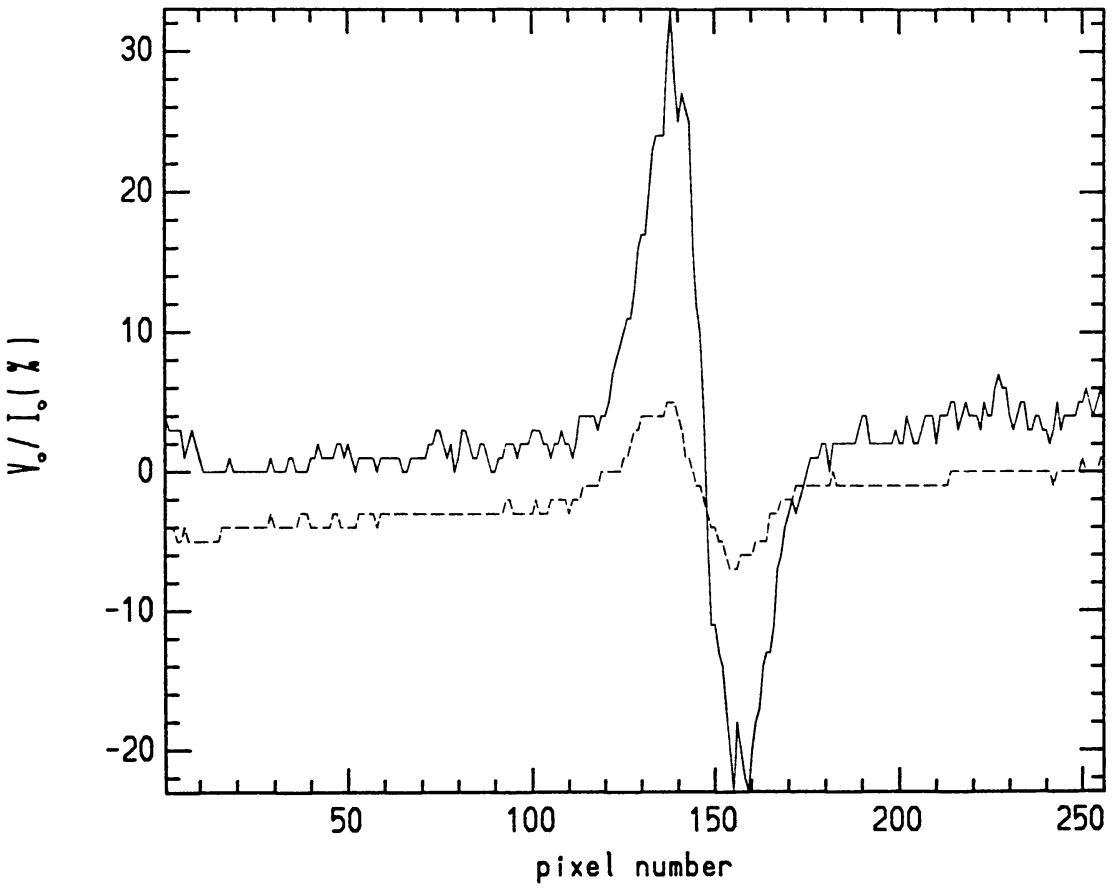


Fig. 5. The profile of circular polarisation ($V_0/I_0$) variation with pixel number at two different positions of a sunspot. The offset in continua of the curves shows the dependence of the measured degree of telescope polarisation in the continuum on the total light, as reflected in columns 6, 7, and 8 of Table I.

being $\leq \pm 1\%$, we can extrapolate a $3\sigma$ detection limit of 500 G, assuming that the field is entirely pointing in the line of sight. Further assumption of a square root scaling of linear polarisation with magnetic field allows us to expect at $3\sigma$ a limit of 1500 G for the transverse field. The binning of 25 spatial pixels will lower these limits to 100 and 300 G, respectively. The use of the systematic profile variation would reduce these limits still further.

The main emphasis of our instrument development has been to integrate available and affordable components into a system that can conveniently measure the magnetic fields of sunspots. Although systematic measurements on sunspots are yet to be performed, the present study indicates that several important problems on the morphological evolution of sunspot fields can be investigated using this instrument in its present stage of development.

## Acknowledgements

We are thankful to the SERC, Department of Science and Technology and Professors K. R. Sivaraman and R. Cowsik for their unstinting support. We are also grateful to Mr A. V. V. Kutty and N. Jayavel from the electronics department for their contribution to the project. The help rendered by the personnel at our Institute's workshops at Bangalore and Kodaikanal, as well as by the observing assistants at the solar tunnel telescope at Kodaikanal, is acknowledged.

## References

Ai, G.: 1987, *Publ. Beijing Astron. Obs.* **9**, 27.
Balasubramaniam, K. S., Venkatakrishnan, P., and Bhattacharyya, J. C.: 1985, *Solar Phys.* **99**, 333.
Bappu, M. K. V.: 1967, *Solar Phys.* **1**, 151.
Hagyard, M. J., Cumings, N. P., West, E. A., and Smith, J. F.: 1982, *Solar Phys.* **80**, 33.
Harvey, J. W.: 1984, in M. J. Hagyard (ed.), *Measurements of Solar Vector Magnetic Fields*, NASA CP-2374, p. 173.
Jones, H. P., Durall, T. L., Jr., Harvey, J. W., Mahaffey, C. T., Schwitters, J. D., and Simmons, J. E.: 1992, *Solar Phys.* **138**, 211.
Lites, B. W., Elmore, G., Murphy, G., Skumanich, A., Tomczyk, S., and Dunn, R. B.: 1991, in L. J. November (ed.), *Solar Polarimetry*, Proceedings of the 11th NSO Summer Workshop, Sunspot, NM, p. 3.
Lundstedt, H., Johannesson, A., Scharmer, G., Stenflo, J. O., Kusoffsky, U., and Larsson, B.: 1991, *Solar Phys.* **132**, 233.
Makita, M., Hamana, S., and Nishi, K.: 1984, in M. J. Hagyard (ed.), *Measurements of Solar Vector Magnetic Fields*, NASA CP-2374, p. 173.
Mickey, D. L.: 1985, *Solar Phys.* **97**, 233.
Rust, D. M. and O'Byrne, J. W.: 1991, in L. J. November (ed.), *Solar Polarimetry*, Proceedings of the 11th NSO Summer Workshop, NM, p. 74.
Skumanich, A. and Lites, B. W.: 1987, *Astrophys. J.* **322**, 473.
Title, A. M., Tarbell, T. D., and Topka, K. P.: 1987, *Astrophys. J.* **317**, 892.
Zirin, H.: 1985, *Australian J. Phys.* **38**, 961.